Pharm Res (2014) 31:566–578
DOI 10.1007/s11095-013-1181-6

RESEARCH PAPER

Preparation, Characterization, and Evaluation of Dipfluzine–Benzoic Acid Co-crystals with Improved Physicochemical Properties

Yulong Lin • Huan Yang • Caiqin Yang • Jing Wang

Received: 29 May 2013 / Accepted: 9 August 2013 / Published online: 25 September 2013

ABSTRACT

Purpose To prepare and characterize the co-crystal of dipfluzine and benzoic acid. To investigate the feasibility of the co-crystal for improving solubility and a faster dissolution rate *in vitro* and evaluate the bioavailability and tissue distribution of co-crystal *in vivo*.

Methods A novel dipfluzine–benzoic acid co-crystal prepared using the solvent-assisted co-grinding and the solvent ultrasonic methods were identified and characterized by powder X-ray diffraction (PXRD), differential scanning calorimetry (DSC) and thermogravimetric analysis (TGA), as well as Raman, solid-state nuclear magnetic resonance (ssNMR), and terahertz (THz) spectroscopy. Pharmacokinetics and tissue distribution were tested *in vivo* using murine models. Statistics analysis for dissolution data of co-crystal *in vitro* and animal experiment data *in vivo* were evaluated using *t*-test.

Results Results of PXRD and DSC identified the dipfluzine–benzoic acid co-crystals were formed with a molar ratio of 1:2. The IR, Raman, and ssNMR spectra verified the formation of O-H···O and O-H···F hydrogen bonds. The complex constant, K, was evaluated to be 10^9 orders of magnitude with $\Delta_r G < 0$. The co-crystal solubility, the rate of drug dissolution and the relative bioavailability were approximately 500 times, five times and double that of dipfluzine, respectively. Increased solubility of co-crystal did not reduce distribution in the brain; the mean concentrations in the brain increased, but the differences had no statistic significance ($p > 0.05$).

Conclusions The co-crystal of dipfluzine–benzoic acid improved the physicochemical properties of dipfluzine, such as solubility and dissolution rate. Furthermore, the increased relative bioavailability of co-crystal indicated the potential use in further clinical study

KEY WORDS bioavailability · co-crystal · dipfluzine · thermodynamic · THz spectra

ABBREVIATIONS

APIs	Active pharmaceutical ingredients
BA	Benzoic acid
CP	Cross-polarization
Dif	Dipfluzine
DSC	Differential scanning calorimetry
FT-IR	Fourier-transform infrared
MAS	Magic-angle spinning
PXRD	Powder X-ray diffraction
SD	Spraque–Dawley
ssNMR	Solid-state nuclear magnetic resonance
TGA	Thermogravimetric analysis
THz	Terahertz
TPPM	Two pulse phase modulation

INTRODUCTION

Generally, the bioavailability of orally administered drugs significantly depends on the solubility and dissolution rate of a drug *in vitro*. Therefore, obtaining the desired solubility and dissolution behavior of drugs is one of the most challenging tasks in designing new forms of drugs. However, most drugs that have been approved since 1995 have poor solubility, poor permeability, or both (1,2). Crystal engineering offers several methods to improve the solubility and dissolution rate of active pharmaceutical ingredients (APIs), such as complexation and co-crystal formation (3–7). The formation of crystalline molecular complexes and co-crystals involves the incorporation of an API with another pharmaceutically acceptable small molecule in the crystal lattice to obtain a distinct physicochemical profile, which could potentially improve the

Electronic supplementary material The online version of this article (doi:10.1007/s11095-013-1181-6) contains supplementary material, which is available to authorized users.

Y. Lin • H. Yang • C. Yang • J. Wang (✉)
School of Pharmaceutical Sciences, Hebei Medical University
Shijiazhuang 050017, China
e-mail: jingwang@home.ipe.ac.cn

properties of API, such as the solubility, dissolution rate, and even bioavailability.

Several techniques are used to characterize the solid-state properties of drug samples at the intramolecular, intermolecular, and lattice levels; these methods include powder X-ray diffraction (PXRD), thermal analysis, Fourier-transform infrared (FT-IR) spectroscopy, Raman spectroscopy, and solid-state nuclear magnetic resonance (ssNMR) spectroscopy (8,9). The use of terahertz (THz) spectroscopy in the study of solid APIs has recently received more attention (10,11). Terahertz radiation (0.1 THz to 3 THz, which corresponds with 3.3 cm^{-1} to 100 cm^{-1}) can induce low-frequency vibrations. The ability of THz spectroscopy to probe lattice and π-π interactions, as well as van der Waals forces and hydrogen-bonding vibrations, makes it a powerful tool for investigating pharmaceutical polymorphisms and crystal solid APIs. We have applied THz spectroscopy in our previous studies to differentiate the different forms of APIs (12,13) and to verify the formation of the azelnidipine–maleic acid complex (14).

Dipfluzine (Fig. 1) is a novel, poorly water-soluble diphenylpiperazine Ca^{2+} channel blocker that was synthesized by the Pharmaceutical School of Hebei Medical University (15). Compared with its analog cinnarizine, dipfluzine effectively induces selective cerebrovascular dilation, reduces thrombosis, lowers cerebral edema, ameliorates or protects rats from ischemic brain injury, and significantly repairs memory impairment caused by sodium nitrite in mice (16,17). Dipfluzine possesses potential anti-arrhythmic activities. To improve the solubility of the drug in water, the effect of dipfluzine–hydrochloric acid complexation on the solubility of dipfluzine in water has been investigated (18). Dipfluzine–hydrochloric acid has higher solubility in water than its base compound dipfluzine, but its acidity and water absorption (hygroscopic weight gain was 1.9±0.2%) limits the applications of the complex. Improving the physical properties of dipfluzine–hydrochloric acid by complexing with co-crystal formers (CCFs) was attempted. Unfortunately, only benzoic acid formed new phase with dipfluzine–hydrochloric acid (19); obviously, the acidity of dipfluzine–hydrochloric acid could not be decreased by complexing with acidic CCF. The present study aimed to investigate the feasibility of forming a complex of base dipfluzine, not dipfluzine–hydrochloric acid, and a weak acid for preparing a novel complex with improved solubility and a faster dissolution rate *in vitro* and to evaluate the bioavailability and tissue distribution *in vivo*.

MATERIALS AND METHODS

Materials

Bulk dipfluzine powder (1-diphenylmethyl-4-[3-(4-fluorobenzoyl)propyl] piperazine) was kindly supplied by the School of Pharmaceutical, Hebei Medical University, and purified by recrystallization in ethanol (20). All other reagents were of analytical grade. Male Spraque–Dawley (SD) rats (Certificate No.13020905), weighing (250±50) g, were obtained from the Experimental Animals Center of Hebei Province (Shijiazhuang, China).

Preparation of Dipfluzine–Benzoic Acid Co-crystals

Solvent-assisted co-grinding method (mainly used): The complexes were prepared by grinding mixtures of dipfluzine and benzoic acid in a carnelian mortar at different dipfluzine/

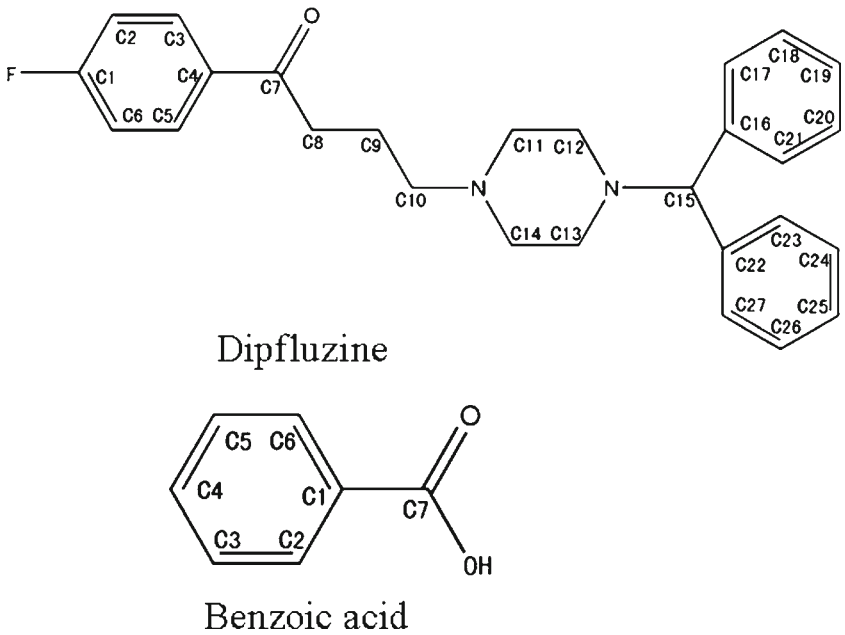

Fig. 1 Chemical structures of dipfluzine and benzoic acid.

benzoic acid ratios of 1:2, 1:1, and 2:1. During grinding, ethanol was added dropwise into the mixtures to form slurries. The amount of ethanol was controlled according to the slurry state. That is, the slurry, neither suspension nor powder, should be maintained at the whole grinding procedure by dropping appropriate amount of ethanol. The samples were collected at different time intervals (10, 30, and 60 mins) and subsequently characterized.

Solvent ultrasonic method: The ultrasonic solution was prepared by dissolving dipfluzine and benzoic acid at 1:1, 1:2, and 2:1 molar ratio in 5 mL anhydrous ethanol in a 10 mL vial. The vials were tightly capped and put into ultrasonic condition at 50°C for 2 h. Then, the ultrasonic solution was cooled to room temperature and put into refrigerator. Separated co-crystal samples were collected and dried in vacuum desiccator

Characterizations

The PXRD profiles were measured on an X-ray diffractometer (RINT 2100 Ultima, Rigaku Co., Japan) using a Cu-K_α target with a 0.3 mm receiving slit, operating at 20 kV and 20 mA. The data were collected within the range of 3° to 40° (2θ) with a step size of 0.05°. Approximately 50 mg of sample powder was carefully loaded into a glass holder, and the sample surface was flattened softly to avoid particle orientation.

The FT-IR spectra were obtained from 4,000 cm^{-1} to 400 cm^{-1} using an Equinox 55 FT-IR spectrometer (Bruker). Each spectrum was the average of 40 separate scans with a spectral resolution of 2 cm^{-1}. The samples were obtained by mixing and grinding 4 mg pure sample with 160 mg IR-grade KBr in an agate mortar.

The Raman spectra were obtained in the range of 40 cm^{-1} to 4,000 cm^{-1} range using a Bruker spectrometer equipped with a 647.1 nm mixed argon–krypton laser (50 mW).

DSC and TGA were performed using a Perkin-Elmer DSC apparatus (Diamond DSC) and Perkin-Elmer TG apparatus (Pyris 1 TG), respectively. The scans were operated within the range of 30°C to 400 C, at a heating rate of 5°C/min to investigate the heating behavior of the co-crystal. Aluminium pans were used as containers (6 mm diameter× 2 mm) and sealed using aluminium lid. Nitrogen, at the flow rate of 20 mL/min, was used as the purging gas, at a flow rate of 20 mL/min.

The THz spectra were acquired using a TPI™ spectra 1,000 transmission spectrometer (TeraView Limited, Cambridge, UK). The samples were measured with an instrument resolution of 2 cm^{-1} to 3 cm^{-1} over the range of 0 THz to 3 THz, which corresponds to 0 cm^{-1} to 100 cm^{-1}.

The solid-state ^{13}C cross-polarization(CP)/magic-angle spinning (MAS) spectra of dipfluzine, benzoic acid, and the dipfluzine–benzoic acid co-crystal were obtained using a Varian Infinity Plus 300 spectrometer (75.40 MHz for ^{13}C, USA) with a variable amplitude CP (2.0 ms contact time). The samples were packed into a 4 mm rotor and spun at a rate of 10.0 kHz. The CP/MAS TPPM (two pulse phase modulation) sequence was used for heteronuclear decoupling during acquisition with a proton field H_{1H} that satisfied the equation: $\omega_{1H}/2\pi=\gamma_H H_{1H}=60$Hz. The recycling time was 5.0 s. Several scans were recorded for each compound to obtain an adequate signal-to-noise ratio. All ssNMR experiments were performed at room temperature.

Solubility of Dipfluzine in Benzoic Acid Solution and Thermodynamic of Co-crystal Formation

The solubility of dipfluzine in benzoic acid at different concentrations was determined at 25, 31, and 37°C. The benzoic acid stock solution was prepared by dissolving 61 mg benzoic acid in 30% ethanol solution in a 100 mL volumetric flask. This solution was further diluted in 30% ethanol solution to obtain the concentrations of 0, 0.5, 1.0, 1.5, and 2 mM. An excess amount of dipfluzine was then placed in 10 mL screw-capped vials with benzoic acid solutions of different concentrations in each. The vials were tightly capped and shaken at 100 rpm in a water bath for 72 h. The concentration of dipfluzine in each solvent was measured by HLPC after filtration through a 0.45 μm membrane filter. Each test was repeated three times; the obtained values were used to calculate the complex constant and the thermodynamic parameters of co-crystal formation.

As confirmed by PXRD (*vide infra*), the stoichiometric ratio of dipfluzine/benzoic acid in co-crystal was 1:2. When an excess amount of dipfluzine (Dif) is added into the solution of benzoic acid (BA), the following equilibrium exists

$$Dif(aq) + 2BA(aq) \leftrightarrow Dif-BA_2(aq) \qquad K = \frac{[Dif-BA_2]}{[Dif][BA]^2} \tag{1}$$

where [Dif–BA_2] and [BA] are the equilibrium concentrations of Dif–BA_2 and BA, respectively; [Dif] is the saturated concentration of Dif; K is the complex constant.

The concentration of Dif (designated as c), which is determined by HPLC, is the sum of [Dif –BA_2] and [Dif]:

$$c = [Dif-BA_2] + [Dif] \tag{2}$$

When the initial concentration of BA is c_0, then:

$$[BA] = c_0 - 2[Dif-BA_2] = c_0 - 2(c-[Dif]) \tag{3}$$

By combining Eqs. (1), (2), and (3), the following equation is derived:

$$K = \frac{c-[Dif]}{[Dif](c_0-2([Dif]))^2} \quad (4)$$

When the concentrations of Dif (c) in different concentrations of BA (c_0) are known, a curve can be drawn with (c) as the y-coordinate and (c_0) as the abscissa:

$$y = ax + b$$

where a and b are the slope and y-intercept of the curve, respectively, and

$$y = c, x = c_0$$

Given that [Dif] is the saturated concentration of Dif, then:

$$[Dif] = b$$
$$K = \frac{y-b}{b(x-2(y-b))^2} = \frac{y-b}{bx^2(1-2a)^2}$$

Subsequently,

$$\frac{y-b}{b} = x^2(1-2a)^2K \quad (5)$$

A curve is then drawn with $\frac{y-b}{b}$ as the y-coordinate and $x^2(1-2a)^2$ as the abscissa. The value of K can be obtained from the slope of this curve.

Subsequently, according to the Van't Hoff equation:

$$lnK = -\frac{\Delta_r H^\theta}{RT} + \frac{\Delta_r S^\theta}{R} \quad (6)$$

A curve is drawn with $\ln K$ as the y-coordinate and $1/T$ as the abscissa. The values of $\Delta_r H^\theta$ and $\Delta_r S^\theta$ can be obtained from the slope and intercept of this curve, respectively.

$\Delta_r G^\theta$ can be calculated using the equation:

$$\Delta_r G^\theta = \Delta_r H^\theta - T\Delta_r S^\theta \quad (7)$$

Stability Experiment

In order to evaluate the stability of co-crystal, the co-crystal was monitored up to 15 days at constant temperature and relative humidity (40°C/75% RH). Periodically (initial, 7 and 15 days) samples were removed and characterized by PXRD studies.

HPLC Operation Conditions

The HPLC analysis was performed at room temperature using Diamonsil™ C18 analytic column (250 mm × 4.6 mm, 5 μm, VWD) with a mobile phase of methanol–water (70:30, v/v) at a flow rate of 1.0 mL/min at a column temperature of 30°C.

Standard stock solutions of dipfluzine were prepared by dissolving the standards in ethanol to a final concentration of 610 μg/mL. This dipfluzine stock solution was diluted using 30% ethanol to obtain the working solutions for the calibration standards at the concentrations of 0.4, 25, 50, 100, 150, 200, and 250 μg/mL. An injection volume of 20 μL was used. The detection wavelength in the UV-visible range was set at 244 nm. The linear ranges were determined to be 0.4 μg/mL to 250 μg/mL using standard injections. The obtained calibration curve with the abovementioned operating conditions was $S = 43.88c + 3.534$, ($r = 0.9999$), where S is the peak area and c is the dipfluzine concentration.

Equilibrium Solubility and Dissolution Rate *In Vitro*

An excess amount of dipfluzine was placed in a 25 mL screw-capped vial with deionized water. The vials were tightly capped and shaken at 100 rpm in the respective water baths at 25, 31, and 37°C for 72 h. The dipfluzine concentration was measured by HLPC after filtration through a 0.45 μm membrane filter.

The dissolution data of the dipfluzine–benzoic acid system were measured using a dissolution tester (RC-3; Guoming, China). Exactly 30 mg pure dipfluzine, a 1:2 physical mixture of dipfluzine and benzoic acid, and the co-crystal equivalent to 30 mg dipfluzine were placed in a dissolution tester containing 900 mL of the dissolution medium (NaAc–HAc buffer solution, pH = 4.5) at (37 ± 0.5)°C (using the paddle method at 100 rpm). Samples were collected at fixed time intervals and immediately replaced with an equal volume of the dissolution medium. The collected receptor medium was filtered with a syringe (pore size = 0.45 μm) and drug content was evaluated. Each test was repeated three times. Kinetic modeling was performed based on nonlinear regression to investigate the drug dissolution mechanism of the co-crystal (12).

Pharmacokinetic Dynamics and Tissue Distribution *In Vivo*

Animals and Sampling

The rats were kept in an environmentally controlled breeding room for three days before starting the experiments. The animals were fed with standard laboratory food and water *ad libitum* and subsequently fasted for 12 h before dosing.

A set of 12 male SD rats were randomly divided into two groups. The intragastric suspensions were prepared by

suspending 500 mg dipfluzine or the co-crystal (equivalent to 500 mg dipfluzine) in 100 mL of 5% sodium carboxymethyl cellulose, then, were orally administered to the respective groups using a single dose of 40 mg/kg. About 0.5 mL blood samples were obtained from each rat at the set time points after intragastric administration from the eye canthus and collected into the respective 1.5 mL heparinized plastic centrifuge tubes. The concentration of dipfluzine in the blood samples was determined by HPLC using liquid–liquid extraction under alkaline conditions after protein precipitation with methanol (21).

Another set of 36 male SD rats were randomly divided into two groups. The suspensions of dipfluzine or the co-crystal were orally administrated to the respective groups at a single dose of 40 mg/kg. The rats were euthanized by cervical dislocation at 1, 6, and 24 h after drug administration. The heart, liver, lungs, kidney, brain, stomach, pancreas, and intestines were immediately collected, dried on filter paper, and stored at - 20°C until further analysis. The concentration of dipfluzine in the tissue samples were determined using liquid–liquid extraction under alkaline conditions after protein precipitation with methanol by HPLC.

Pharmacokinetic Analysis

All pharmacokinetic parameters were calculated with one-compartmental model ($1/c^2$) using the 3P97 software program (Mathematical Pharmacology of Chinese Society), including the time point of maximum plasma concentration (T_{max}), maximum plasma concentration (C_{max}), apparent volume of distribution (V), clearance (CL), elimination rate constant (k_e), and elimination half-life ($t_{1/2}$), as well as the area under the plasma concentration–time curve (AUC). The relative bioavailability of the co-crystal to dipfluzine was calculated as $(AUC)_{co\text{-}crystal}/(AUC)_{dipfluzine}$.

Statistical Analysis

Dissolution data of co-crystal *in vitro* and animal experiment data *in vivo* were analyzed by *t*-test using SPSS 13.0 software program (Statistical Product and Service Solutions Company, U.S.). A 0.05 level of probability was taken as the minimal level of significance.

RESULTS AND DISCUSSION

Physicochemical Characterization of the Dipfluzine–Benzoic Acid Co-crystals

PXRD patterns and DSC

The solvent-assisted grinding method was initially used to produce the dipfluzine–benzoic acid co-crystals at different dipfluzine/benzoic acid ratios and different grinding times. The PXRD patterns of the different dipfluzine–benzoic acid systems are presented in Figs. 2, 3 and 4. When dipfluzine was

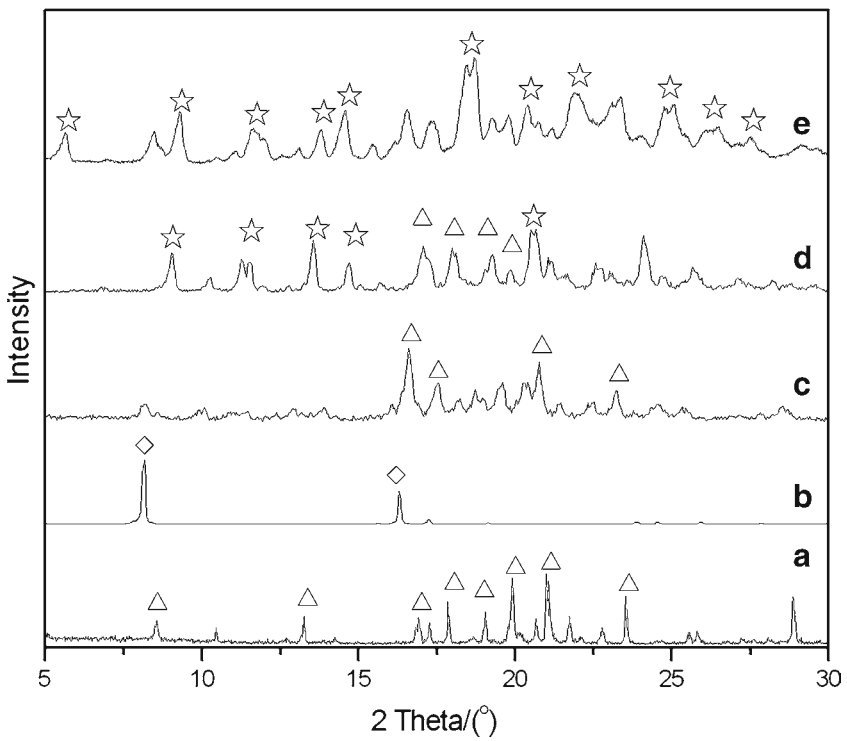

Fig. 2 PXRD patterns of dipfluzine–benzoic acid system after grinding for 60 min: (**a**) dipfluzine; (**b**) benzoic acid; (**c**) dipfluzine/benzoic acid at 2:1; (**d**) dipfluzine/benzoic acid at 1:1; (**e**) dipfluzine/benzoic acid at 1:2 (Δ: dipfluzine, ◇: benzoic acid, ☆: new peaks for the co-crystals)

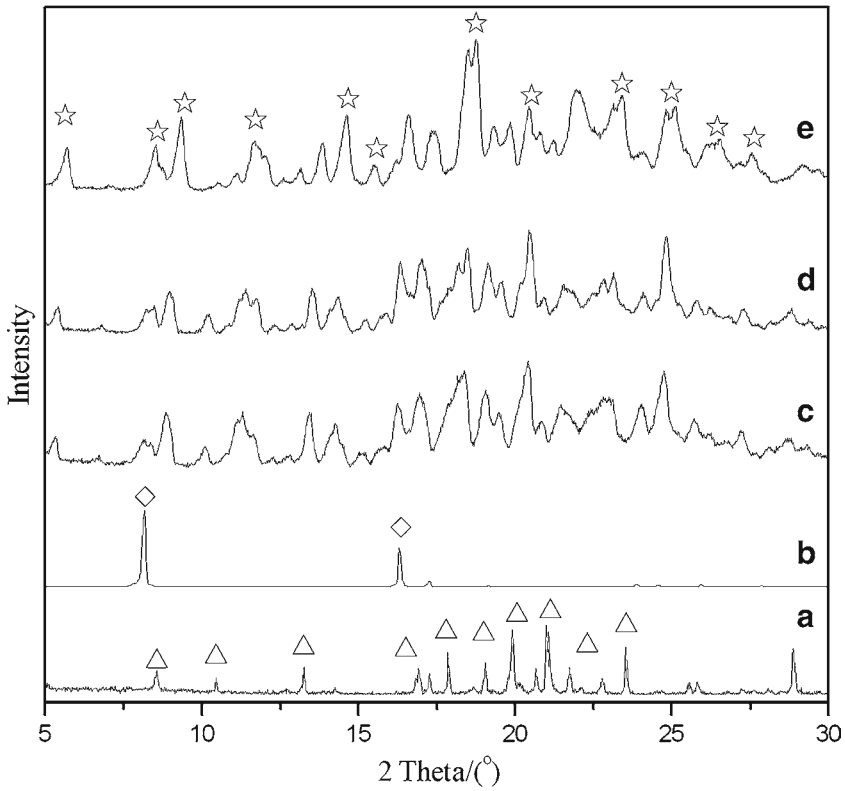

Fig. 3 PXRD patterns of (**a**) dipfluzine, (**b**) benzoic acid, and the co-crystals of dipfluzine–benzoic acid at molar ratio of 1:2 after grinding at different time intervals: (**c**) 10 min; (**d**) 30 min; (**e**) 60 min (Δ: dipfluzine, ◇: benzoic acid, ☆: new peaks for the co-crystals).

ground with benzoic acid at a dipfluzine/benzoic acid molar ratios of 1:1 or 2:1, new peaks were observed other than those corresponding to the excess amounts of the starting components (Figs. 2c and d), which indicated that the dipfluzine/benzoic acid molar ratios of 1:1 and 2:1 were unsuitable stoichiometries for co-crystal formation. Meanwhile, additional new PXRD peaks were observed for the complex with the 1:2 ratio (Fig. 2e). The positions of the new peaks were

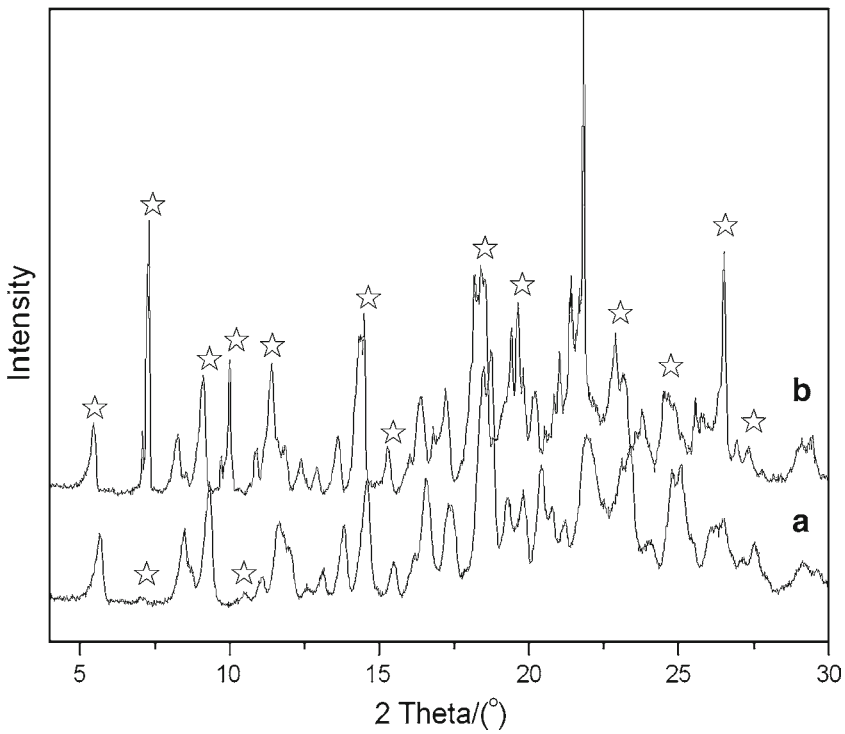

Fig. 4 PXRD patterns of dipfluzine–benzoic acid co-crystal synthesized by different methods: (**a**) solvent-assisted grinding method; (**b**) solvent ultrasonic method (☆: new peaks for the co-crystal).

apparently different from those of the starting components, thereby suggesting that the complex between dipfluzine and benzoic acid was presumably formed from the 1:2 molar ratio by solvent-assisted co-grinding.

The complex formation between dipfluzine and benzoic acid apparently easily occurred within a short grinding time (Fig. 3c). Compared with intact dipfluzine and benzoic acid, the PXRD peak intensity of co-crystal was decreased, indicating that co-crystal formation decreased the crystallinity of material and some amorphous material may be present (Figs. 3a to c). Compared PXRD pattern of 10 min-grinding co-crystal with those of 30 and 60 min -grinding co-crystals, grinding did not decrease the crystallinity of co-crystal but favored the crystalloid growth (Figs. 3d to e).

Co-crystals with same crystal structure can generally be synthesized by different methods, if co-crystal can be formed between an API and a CCF. To validate the regularity of the co-crystal formation, a solvent ultrasonic method was used to produce the co-crystal with a dipfluzine/benzoic acid molar ratio of 1:2 in addition to the solvent-assisted co-grinding method. The contrasting PXRD patterns of the samples prepared by different methods are compared in Fig. 4. The same peaks were observed in both PXRD patterns, thereby indicating that the same complex was produced by the two different methods. Slight discrepancies in the peak locations and intensities were observed, which were presumably attributed to the preferred orientation effects of the different shapes and sizes of the particles in the microcrystals prepared by different methods.

The thermal behaviors of dipfluzine and the co-crystals produced using different methods were investigated by DSC and TGA and the resulting curves are shown in Fig. 5. The intact dipfluzine crystal had an endothermic peak because of melting at 137°C and an exothermic peak because of decomposition at approximately 310°C.

The DSC curves for the co-crystals of both solvent-assisted co-grinding and solvent ultrasonic methods had lower melting points and decomposition temperatures. Thus, these co-crystals had different crystal structures, as compared with the intact dipfluzine. The fusion temperature of the co-crystal was below 100°C, which is significantly lower than those of intact dipfluzine (137°C) and benzoic acid (122°C). According to the survey of Schultheiss and Newman (22), 39% cocrystalline samples had melting points lower than either the API or CCF. Dipfluzine-benzoic acid co-crystal contributed to this group. The single melting point in the DSC curve of the co-crystal from the dipfluzine/benzoic acid ratio of 1:2 resulted from a complex, that is, the co-crystal of dipfluzine–benzoic acid. Therefore, the obtained co-crystal was formed according to the initial ratio of 1:2. Meanwhile, the co-crystals experienced two-stage decomposition procedures after melting. Dipfluzine-benzoic acid co-crystal with molar ratio of 1:2 contains 36.96% benzoic acid by weight, which appears to coincide with the first weight loss stage of the TG curve. After co-crystal melted, the hydrogen bonds in co-crystal were

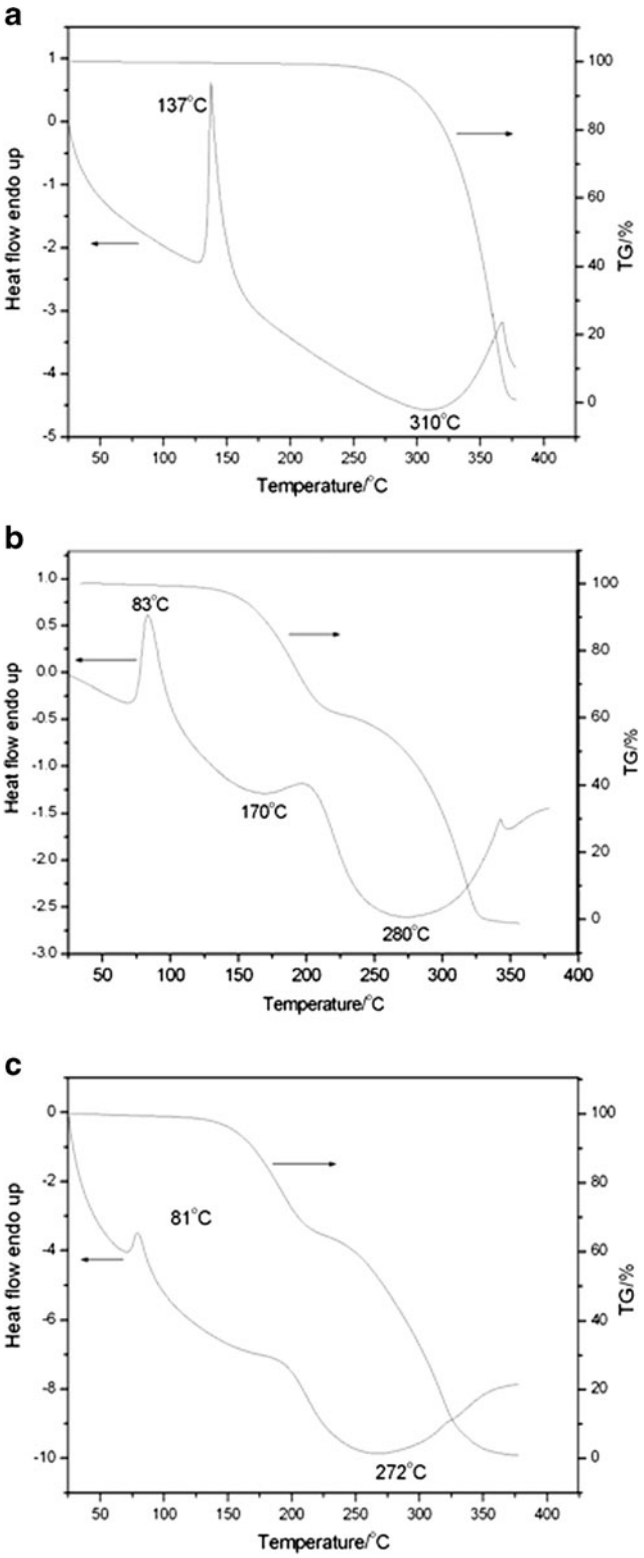

Fig. 5 DSC and TG curves for dipfluzine–benzoic acid system: (**a**) dipfluzine; (**b**) dipfluzine–benzoic acid co-crystal prepared by solvent-assisted co-grinding; (**c**) dipfluzine–benzoic acid co-crystal prepared by solvent ultrasonic method.

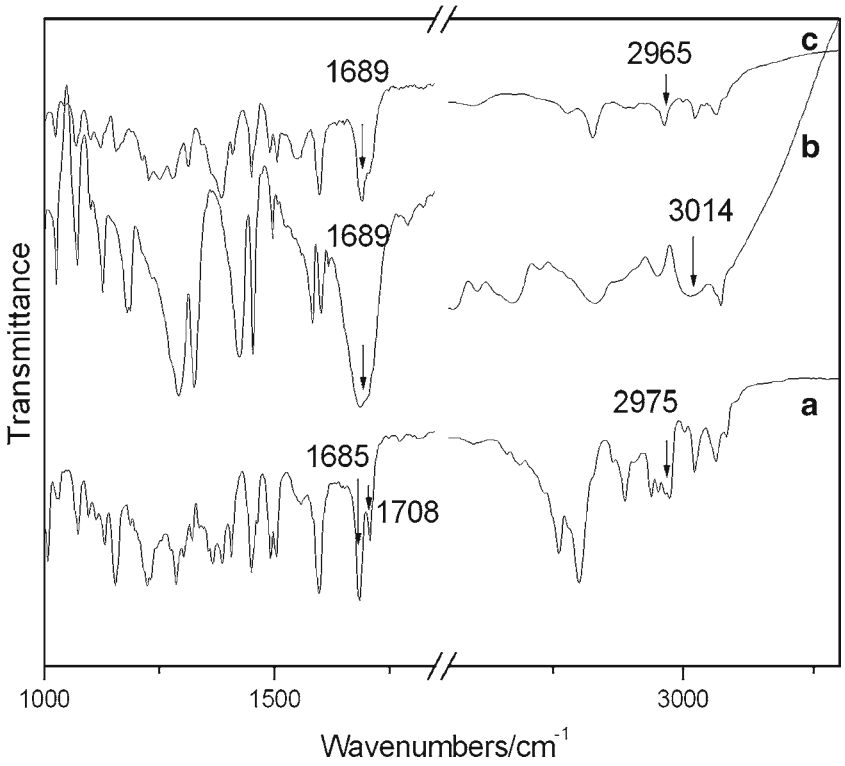

Fig. 6 IR spectra of dipfluzine–benzoic acid system after grinding for 60 min: (**a**) dipfluzine; (**b**) benzoic acid; (**c**) dipfluzine/benzoic acid, 1:2.

destroyed; easily sublimated benzoic acid sublimated in the first-stage decomposition procedure. Whereas the exothermic peak at approximately 200°C to 330°C was due to the decomposition of the intact dipfluzine. The final dipfluzine–benzoic acid co-crystal stoichiometry was approximately 1:2 within the detection limits of PXRD and DSC.

FT-IR Spectra

FT-IR, Raman, THz, and ssNMR spectroscopy were performed on the dipfluzine–benzoic acid system to verify the molecular interactions between dipfluzine and benzoic acid in the co-crystal. The FT-IR spectra of dipfluzine,

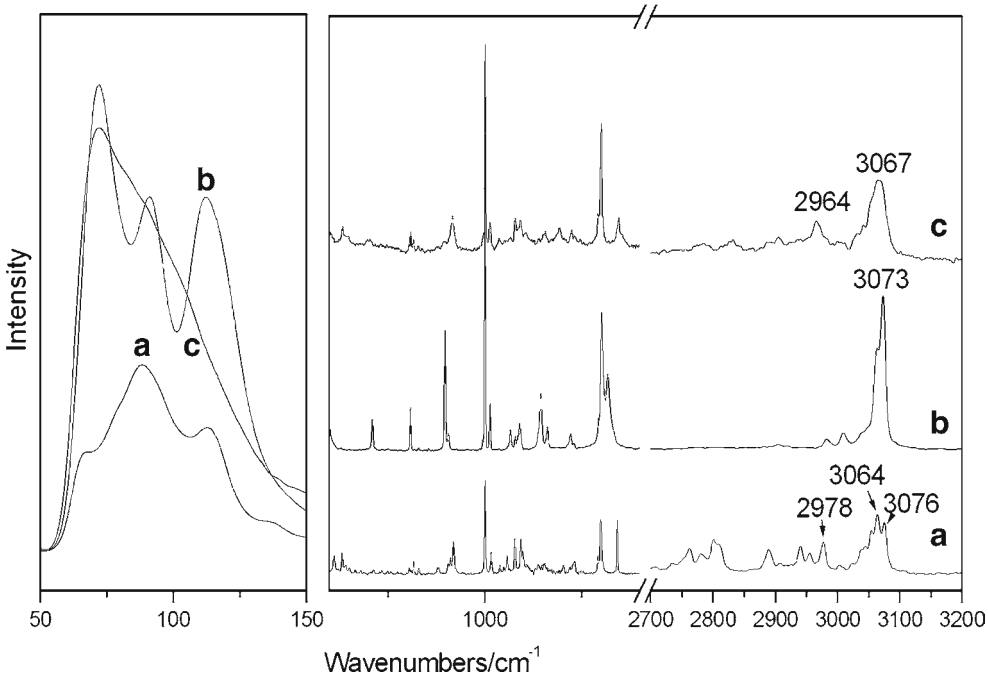

Fig. 7 Raman spectra of dipfluzine–benzoic acid co-crystal after grinding for 60 min: (**a**) dipfluzine; (**b**) benzoic acid; (**c**) dipfluzine/benzoic acid, 1:2.

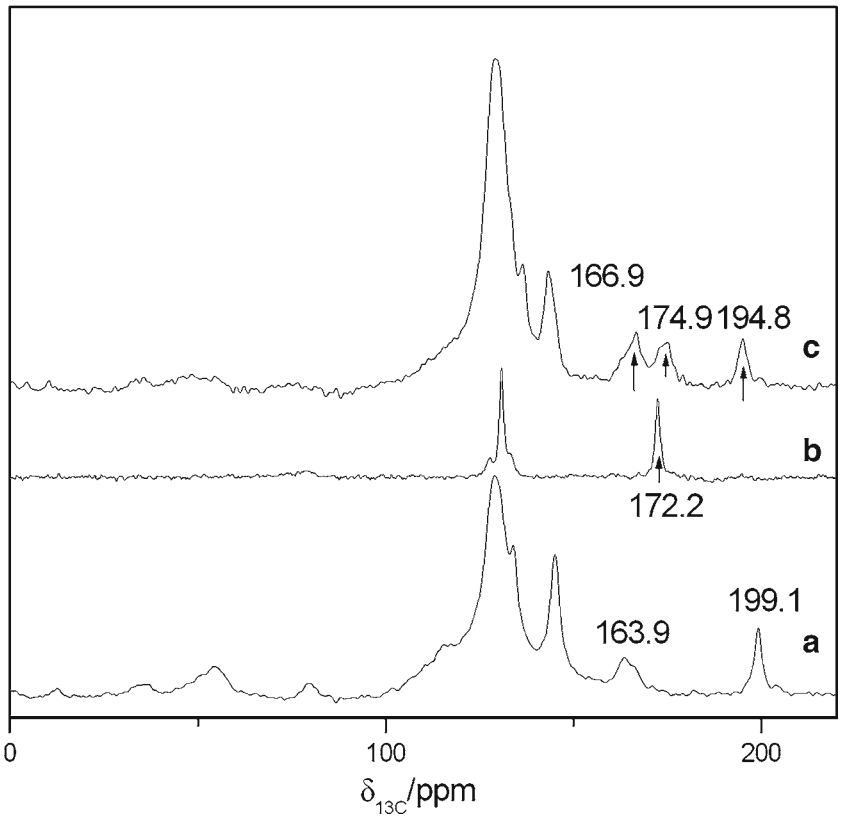

Fig. 8 ssNMR spectra of dipfluzine–benzoic acid co-crystal after grinding for 60 min: (**a**) dipfluzine; (**b**) benzoic acid; (**c**) dipfluzine/benzoic acid, 1:2.

benzoic acid, and dipfluzine–benzoic acid co-crystal are presented in Fig. 6.

The spectra of dipfluzine showed a peak corresponding to the carbonyl (C=O) stretching at 1,685 cm^{-1} (Fig. 6), which overlapped with the carbonyl (C=O) stretching from benzoic acid in the co-crystal. The change of the carbonyl (C=O) vibration in the dipfluzine before and after complex was difficult to verify using the IR spectra alone. The broad band characteristics of benzoic acid at 3,014 cm^{-1}, where O–H valence vibrations occurred, had shifted to 2,965 cm^{-1} in the co-crystal. Thus, the interaction modes of O–H with the surrounding functional groups changed before and after co-crystal formation. The IR vibrations of the hydrogen bond donor and acceptor generally shifted to low wave numbers of 20 cm^{-1} to 50 cm^{-1} after hydrogen bond formation.

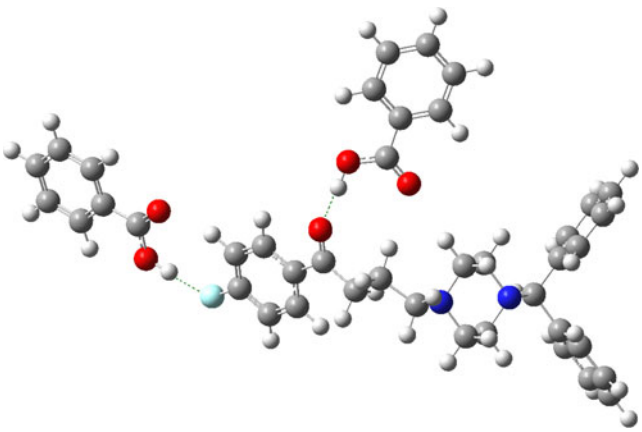

Fig. 9 The simulated plausible model of the interactions between dipfluzine and benzoic acid in co-crystal. Modeling was carried out using GAUSSIAN-03 program package at the DFT B3lyp/6-31G** level.

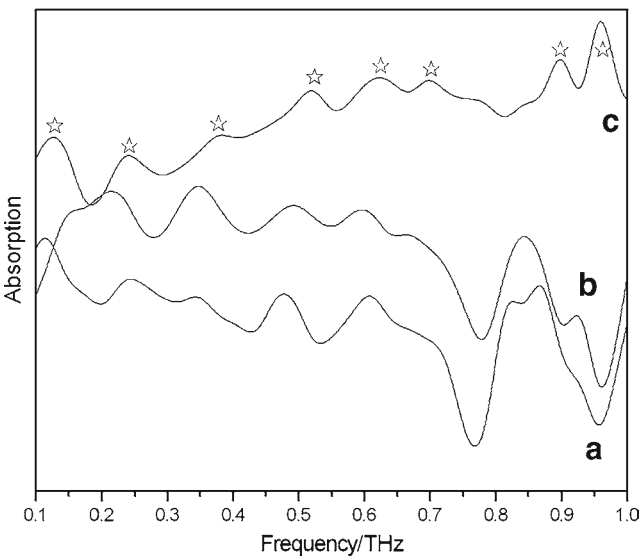

Fig. 10 THz spectra of the dipfluzine–benzoic acid co-crystal after grinding for 60 min: (**a**) dipfluzine; (**b**) benzoic acid; (**c**) dipfluzine/benzoic acid, 1:2.

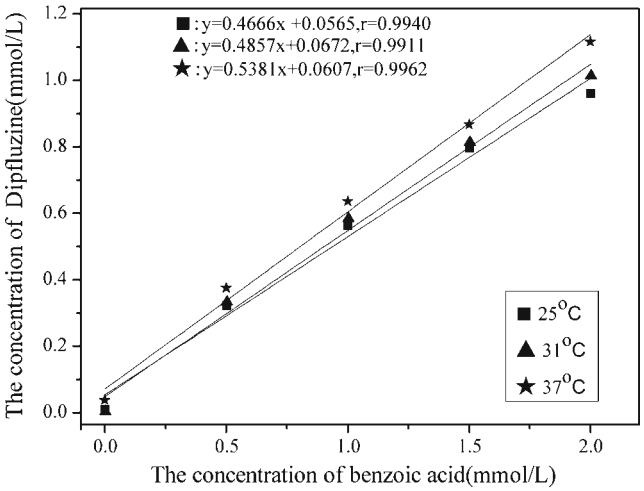

Fig. 11 Curves of dipfluzine concentration versus benzoic acid concentration in 30% ethanol.

Therefore, hydrogen bonds were formed between O–H in benzoic acid and other groups in dipfluzine.

Raman Spectra

The FT-Raman spectra of the dipfluzine–benzoic acid system were depicted in Fig. 7. The spectrum of co-crystal was not simply an overlap of the spectra of its starting components, but was due to the complexation between these compounds. The lattice vibrations in the region below 150 cm^{-1} clearly reflected the different crystal lattices of the intact dipfluzine, benzoic acid, and their co-crystal. Furthermore, the O–H stretching Raman line appeared at 3,073 cm^{-1} in the spectra of benzoic acid and shifted to 3,067 cm^{-1} in the co-crystal.

ssNMR Spectra

To further investigate the intermolecular interaction between dipfluzine and benzoic acid, the ^{13}C CP-MAS ssNMR spectra of the dipfluzine–benzoic acid system were determined and shown in Fig. 8. The comparison between the spectra of benzoic acid and the co-crystal showed that the ^{13}C at position 172.2 ppm, which was assigned to C=O in benzoic acid, shifted to 174.9 ppm in the co-crystal. Thus, the micro-environment of C=O in benzoic acid had changed after co-crystal formation. This shift could be attributed to the change

Table I Complex Constants and Thermodynamic Parameters of Co-crystal Formation

T(K)	K(*10^9 mol^{-1})	$\triangle_r G$(kJ/mol)	$\triangle_r H$(kJ/mol)	$\triangle_r S$(J/mol)
298	4.611	−55.3187	−59.8708	−15.2678
314	3.488	−55.2271		
320	1.806	−55.1355		

Table II Equilibrium Solubility of Dipfluzine and the Co-crystal (μg/mL)

T(K)	Dipfluzine	Cocrystal
298.15	0.2710	161.5
304.15	0.4232	279.6
310.15	0.7219	345.8

in the micro-environment of the neighboring –OH. This result is consistent with the IR analysis. In addition, the comparison between the spectra of dipfluzine and the co-crystal showed chemical shifts of the carbons assigned to C=O and C–F. The ^{13}C at position 199.1 ppm, which was originally assigned to C=O in dipfluzine, had shifted to 194.8 ppm in the co-crystal, whereas the ^{13}C at position 163.9 ppm, which was assigned to C–F in dipfluzine, shifted to 166.9 ppm in the co-crystal. As illustrated in the IR and NMR spectra, the micro-environment of –OH in benzoic acid changed after complexation with dipfluzine. The results suggested that C=O and C–F of dipfluzine interacted with the –OH group in benzoic acid. That is, two benzoic acid molecules were connected to one dipfluzine molecule by hydrogen bonds of –O-H···O and –O-H···F at two positions: the middle carbonyl group and terminal aromatic C–F group. The simulated plausible model of the interaction between dipfluzine and benzoic acid in co-crystal is showed in Fig. 9. The ssNMR spectra provided further evidence of the intermolecular interaction in the co-crystal.

THz Spectra

An overlay of THz spectra for the dipfluzine and benzoic acid systems is shown in Fig. 10. The dipfluzine–benzoic acid co-crystal exhibited several distinct absorption peaks, as compared with those of its starting components. The THz spectra

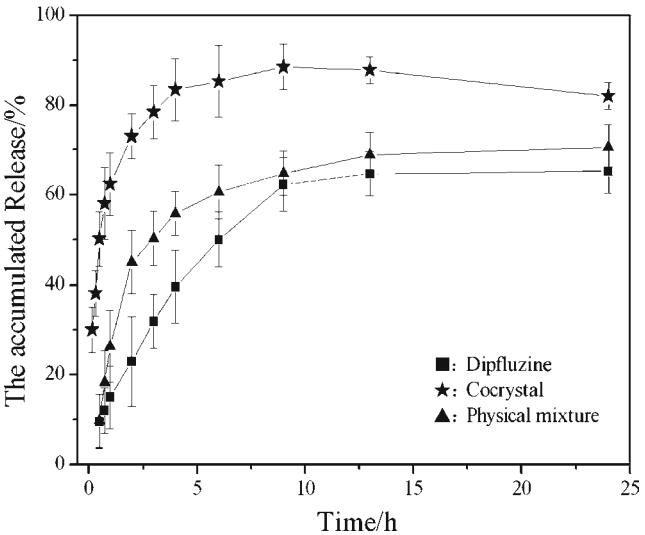

Fig. 12 Dissolution rate of the co-crystal *in vitro* at (37 ± 0.5) °C. $(n = 3, \bar{x} \pm s)$.

Table III Regression Equations of Dipfluzine and the Co-crystal *In Vitro* at (37 ± 0.5) °C

	Regression equation	*R*
Dipfluzine	$Q = 22.64\ t^{1/2}$-7.954	0.9986
Cocrystal	lnln(1/(1-Q%)) = 0.5238lnt-0.0446	0.9974

were highly sensitive to weak intermolecular interactions, such as π-π interactions and hydrogen-bonding stretches, etc., as compared with the IR and Raman spectra. As previously reported by our team, the THz spectra and the density function theory (DFT) calculation can be used to predict weak intermolecular interactions in the two polymorphs of *m*-nisoldipine (13). However, the crystallographic data of the co-crystal was not obtained in the present experiment. Thus, the assignments of THz peaks were difficult to detect by subsequent DFT calculation. Nevertheless, the distinct spectral differences suggested that the dipfluzine–benzoic acid co-crystal was not a simple mixture; it had a novel form with a different crystal stacking structure.

Thermodynamics of Co-crystal Formation

After the characterization of the co-crystal, we attempted to investigate the thermodynamics of co-crystal formation using the solubility method. The temperature-dependent solubility data were collected in 30% ethanol at temperatures of 25, 31, and 37°C. The concentration curves of the dipfluzine and benzoic acid concentrations were assigned as *y*-coordinate and the abscissa, respectively (Fig. 11). The solubility of dipfluzine increased with the benzoic acid concentration, which suggested that the increased solubility of dipfluzine *via* complexation with benzoic acid may improve the properties of the API. Eqs. (5), (6), and (7) were used to calculate the complex constants and thermodynamic parameters, which are listed in Table I. The complex constant K was evaluated to be 10^9 order of magnitude and $\triangle_r G < 0$, thereby indicating the high complexation ability between dipfluzine and benzoic acid in 30% ethanol.

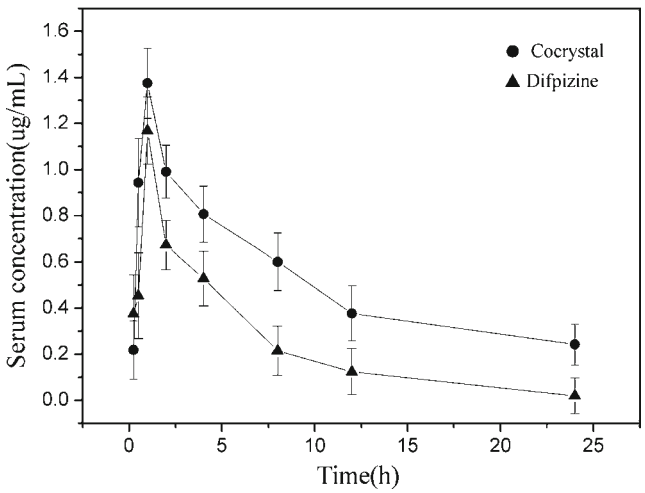

Fig. 13 Mean plasma concentration–time curves of dipfluzine and the co-crystal in rats after oral administration. $(n = 6, \bar{x} \pm s)$.

Table IV Mean Pharmacokinetic Parameters After Oral Administration of Dipfluzine and Co-crystal in Rats (n = 6)

Parameters	Value	
	Dipfluzine	Cocrystal
k_e (1/h)	0.17 ± 0.01	0.10 ± 0.01
T_{lag} (h)	0.03 ± 0.02	0.01 ± 0.01
$t_{1/2}$ (k_e) (h)	4.22 ± 0.26	7.35 ± 1.15
T_{max} (h)	1.05 ± 0.11	0.82 ± 0.13
C_{max} (μg/mL)	0.61 ± 0.09	1.25 ± 0.14
AUC (μgh/mL)	5.16 ± 1.44	14.75 ± 1.60
CL (L/kg/h)	7.65 ± 1.78	2.94 ± 0.48
V (L/kg)	46.43 ± 13.03	28.89 ± 3.34

Stability Study

The results of stability experiment for co-crystal showed that there were no phase transitions after storage condition (40°C/75% RH) for 15 days; the co-crystal was nonhygroscopic, undergoing a weight gain of less than 0.2% at 75% RH (data not show). Although the melting point of co-crystal was low, high complex constant ensured the stability.

Solubility and Dissolution Rate of the Dipfluzine–Benzoic Acid Co-crystal

The equilibrium solubility of dipfluzine and its co-crystal are listed in Table II. Intact dipfluzine was almost insoluble in

Table V Tissue Concentration of Intact Dipfluzine in Rats After a Single Oral Dose of 40 mg/kg (n = 6)

Tissues	Concentration (μg/g)		
	1 h	6 h	24 h
Heart	1.01 ± 0.12	0.57 ± 0.14	0.43 ± 0.07
liver	0.94 ± 0.03	2.46 ± 0.16	0.97 ± 0.18
lung	1.65 ± 0.07	1.10 ± 0.32	0.83 ± 0.05
Kidney	1.07 ± 0.17	2.20 ± 0.21	2.33 ± 0.25
Brain	2.26 ± 0.18	1.42 ± 0.16	0.66 ± 0.08
Pancrea	1.31 ± 0.11	0.87 ± 0.11	0.38 ± 0.34
Stomach	1.34 ± 0.08	0.92 ± 0.05	0.25 ± 0.10
L-intestine	0.53 ± 0.13	1.68 ± 0.18	0.54 ± 0.19
S-intestine	0.96 ± 0.07	1.91 ± 0.16	2.51 ± 0.20

water, whereas the solubility of co-crystal was dramatically improved.

To investigate the dissolution rate of as-prepared complex, the amount of dipfluzine dissolved from the co-crystal was plotted as a function of time (Fig. 12). The t_{50} of intact dipfluzine, the dipfluzine–benzoic acid physical mixture, and the co-crystal were 3.0, 1.4, and 0.48 h, respectively. Compared with intact dipfluzine and physical mixture, the co-crystal showed faster dissolution rate ($p < 0.05$). Therefore, co-crystal formation improved the physicochemical properties such as the dissolution rate. The regression equations of dipfluzine and the co-crystal were fitted with Higuchi and Weibull models, respectively. These regression equations are presented in Table III.

Pharmacokinetic Studies

Bioavailability measures the extent to which a drug reaches the systemic circulation, which is an important index to consider when preparing new forms of an API. Aside from improving the solubility and dissolution rate, the ultimate goal of co-crystal investigation was to improve the bioavailability of an API. The mean plasma concentration–time curves of dipfluzine and co-crystal after oral administration to rats are shown in Fig. 13, and the relevant pharmacokinetic parameters are listed in Table IV.

A "single-peak" was observed in both curves, thereby indicating that both dipfluzine and the co-crystal followed the one-compartment model. Compared with single dipfluzine, the co-crystal showed a smaller elimination rate constant, prolonged elimination half-life, and higher maximum plasma concentration. The AUC of the co-crystal was higher than that of dipfluzine ($p < 0.05$), and the relative bioavailability of the co-crystal to intact dipfluzine was 285.85%. Therefore, the co-crystal provided higher bioavailability than intact dipfluzine.

Table VI Tissue Concentration of the Dipfluzine–Benzoic Acid Co-crystal in Rats After a Single Oral Dose of 40 mg/kg ($n = 6$)

Tissues	Concentration ($\mu g/g$)		
	1 h	6 h	24 h
Heart	1.27 ± 0.10	0.36 ± 0.14	0.33 ± 0.05
liver	0.93 ± 0.03	2.14 ± 0.13	0.88 ± 0.09
lung	1.91 ± 0.14	1.30 ± 0.22	0.75 ± 0.09
Kidney	1.10 ± 0.12	1.64 ± 0.16	2.99 ± 0.25
Brain	2.66 ± 0.13	1.72 ± 0.15	1.33 ± 0.059
Pancrea	1.35 ± 0.14	1.04 ± 0.12	0.31 ± 0.08
Stomach	1.50 ± 0.18	0.75 ± 0.12	0.08 ± 0.09
L-intestine	0.99 ± 0.10	1.32 ± 0.35	0.68 ± 0.13
S-intestine	1.81 ± 0.18	1.34 ± 0.37	0.12 ± 0.10

Tissue Distribution

The tissue distribution of dipfluzine and the co-crystal at different time points are summarized in Tables V and VI. Both dipfluzine and the co-crystal were widely distributed into the tissues, thereby indicating that co-crystal formation did not affect the metabolism and kenosis of dipfluzine. Interestingly, decreased lipophilicity of co-crystal did not reduce distribution in the brain; the mean concentrations in the brain increased, but the differences had no statistic significance ($p > 0.05$)

CONCLUSION

The solvent-assisted co-grinding method can effectively induce co-crystal formation by adding relatively minor amounts of the solvent, which can dissolve or partially dissolve the API and CCF. The facilitation of mechanical stress-induced co-crystal formation in the slurry is explained by the stabilization of the co-crystal in the strong hydrogen-bond network formed between the dipfluzine and benzoic acid molecules. The grinding effect on slurry mixtures could be enhanced by the increased degrees of orientational and conformational freedom made available to the dipfluzine and benzoic acid molecules at the various interfaces, including the liquid–liquid, solid–solid, and solid–liquid interfaces. Consequently, more opportunities for molecular collisions are available.

A novel dipfluzine–benzoic acid co-crystal was prepared by solvent-assisted co-grinding method and characterized by PXRD, DSC, IR, Raman, THz, and ssNMR techniques. The PXRD and DSC results demonstrated that the co-crystal of dipfluzine and benzoic acid was formed at a molar ratio of 1:2. The indications of IR, Raman, and ssNMR showed that C=O and C–F of dipfluzine interacted with the –OH group in benzoic acid. Co-crystals are usually formed through strong hydrogen bonds, particularly between a carboxylic acid and a *N*-heterocyclic hydrogen bond acceptor (23,24). However, the difference between a co-crystal and a salt is that the proton is transferred completely from the acid to the base in a salt, whereas it is only partially transferred in a co-crystal (25). In principle, this event replaces the desired O–H···N hydrogen bond interaction in a co-crystal with a charge-assisted $O\cdots H\text{–}N^{+}$ hydrogen bond in a salt. The single crystal structure of the dihydrochloride monohydrate of dipfluzine was previously resolved, which involved its piperazine ring (26). The piperazine ring in dipfluzine dihydrochloride adopts a chair conformation and both N atoms are protonated. When the hydrochloric acid is replaced by benzoic acid, partial proton transfer would occur because benzoic acid is theoretically not strong enough to induce complete proton transfer. Consequently, the O–H···N hydrogen bond interaction is induced between dipfluzine and benzoic acid. However, the unexpected hydrogen bonds of –

O–H···O and –O–H···F were formed, and not the O–H···N hydrogen bond.

Although hydrogen bond force interactions occurred between dipfluzine and benzoic acid, the complexation force between these molecules was stronger. The co-crystal effectively improved the physicochemical properties of the API, such as solubility and dissolution rate. Furthermore, co-crsytal of dipfluzine-benzoic acid significantly increased the bioavailability of the poorly soluble parent free base dipfluzine, which make it a novel solid form as a potential alternative to pure dipfluzine.

ACKNOWLEDGMENTS AND DISCLOSURES

This work was supported by the Fund of research and development in Science and Technology of Hebei Province of China (12276402D), the National Natural Science Funds of China (NSFC 81202504 and 11204191). The authors would like to express their sincere gratitude to Department of Physics, Capital Normal University, Beijing, China, for the terahertz spectroscopy equipment and School of Chemistry and Material Science, Hebei Normal University, Shijiazhuang, China, for DFT modeling simulation.

REFERENCES

1. Hauss DJ. Oral lipid-based formulations. Adv Drug Deliv Rev. 2007;59(7):667–76.
2. Connors RD, Elder EJ. Using a portfolio of particle growth technologies to enable delivery of drugs with poor water solubility. Drug Deliv Technol. 2004;4(8):78–83.
3. Limwikrant W, Higashi K, Yamamoto K, Moribe K. Characterization of ofloxacin-oxalic acid complex by PXRD, NMR, and THz spectroscopy. Int J Pharm. 2009;382(1–2):50–5.
4. Fand L, Numajiri S, Kobayashi D, Ueda H, Nakayama K, Miyamae H, *et al*. Physicochemical and crystallographic characterization of mefenamic acid complexes with alkanolamines. J Pharm Sci. 2004;93(1):144–54.
5. Blagden N, de Matas M, Gavan PT, York P. Crystal engineering of active pharmaceutical ingredients to improve solubility and dissolution rates. Adv Drug Deliv Rev. 2007;59(7):617–30.
6. Stanton MK, Bak A. Physicochemical properties of pharmaceutical co-crystals: a case study of ten AMG 517 co-crystals. Cryst Growth Des. 2008;8(10):3856–62. doi:10.1021/cg800173d.
7. Schultheiss N, Newman A. Pharmaceutical cocrystals and their physicochemical properties. Cryst Growth Des. 2009;9(6):2950–67.
8. Aaltonen J, Alles M, Mirza S, Koradia V, Gordon KC, Rantanen J. Solid form screening–a review. Eur J Pharm Biopharm. 2009;71(1):23–37.
9. Aaltonen J, Gordon KC, Strachan CJ, Rades T. Perspectives in the use of spectroscopy to characterise pharmaceutical solids. Int J Pharm. 2008;364(2):159–69.
10. Ueno Y, Ajito K. Analytical terahertz spectroscopy. Anal Sci. 2008;24(2):185–92.
11. Taday PF, Bradley IV, Arnone DD, Pepper M. Using terahertz pulse spectroscopy to study the crystalline structure of a drug: a case study of the polymorphs of ranitidine hydrochloride. J Pharm Sci. 2003;92(4):831–8.
12. Li D, Wang M, Yang CQ, Wang J, Ren GD. Solid state characterizations and analysis of stability in azelnidipine polymorphs. Chem Pharm Bull. 2012;60(8):995–1002.
13. Yang CQ, Zhang ZW, Zeng YL, Wang J, Wang YL, Ma BQ. Structures and characterizations of m-nisoldipine polymorphs. CrystEngComm. 2012;14(7):2589–94.
14. Lian WG, Lin YL, Wang M, Yang CQ, Wang J. Crystal engineering approach to produce complex of azelnidipine with maleic acid. CrystEngComm. 2013;15(19):3885–91.
15. Miao QF, Su SW, Zhang W, Guo MF, Li LF, Meng J, *et al*. Effects of dipfluzine on experimental arrhythmias and cytosolic calcium concentration. Chin J Pharmacol Toxicol. 2006;20(6):448–54.
16. Wang C, Zhang YJ, Wang YL. Effects of dipfluzine on delayed afterdepolarizations and triggered activity induced by ouabain in guinea pig papillary muscles. Acta Pharmacol Sin. 2002;23(10):905–9.
17. Zhang YJ, Wang YL, He RR. Effect of dipfluzine on isop renaline induced early afterdepolarizations and triggered activity. Chin J Pharmacol Toxicol. 2000;14(4):318–20.
18. Du YM, Wang YL, Zhang K, Gu JM. The synthesis methods of dipfluzine complex salts, Chinses patent CN101381349A; Mar 11, 2009.
19. Yang CQ, Wang J, Zhang ZW. Synthesis and spectra chatacteristic of pharmaceutical dipfluzine hydrochloride-benzoic acid co-crystal. Spectrosc Spectr Anal. 2011;31(9):2476–9.
20. 20 Wang YL, Chen ZM, Bao CH, Zhang YJ. The synthesis methods of dipfluzine, Chinses patent CN 1326845C; July 18, 2007
21. Jin YH, Preparation and study of dipfluzine intragastric floating and residence sustained-release tablet. Master dissertation, Hebei Medical University. 2004
22. Schultheiss N, Newman A. Pharmaceutical cocrystals and their physicochemical properties. Cryst Growth Des. 2009;9(6):2950–67.
23. Aakeröy CB, Desper J, Scott BMT. Balancing supramolecular reagents for reliable formation of co-crystals. Chem Comm. 2006;13:1445–7.
24. Aakeröy CB, Desper J, Leonard B, Urbina JF. Toward high-yielding supramolecular synthesis: directed assembly of ditopic imidazoles/benzimidazoles and dicarboxylic acids into cocrystals via selective O-H···N hydrogen bonds. Cryst Growth Des. 2005;5(3):865–73.
25. Aakeröy CB, Fasulo ME, Desper J. Cocrystal or salt: does it really matter? Mol Pharm. 2007;4(3):317–22.
26. Wang J, Wang YL, Yang CQ. 1-Diphenylmethyl-4-[3-(4-fluorobenzoyl)propyl]piperazine-1,4-diium dichloride monohydrate. Acta Cryst. 2011;E67(10):o2719.